Lab on a Chip

Accepted Manuscript
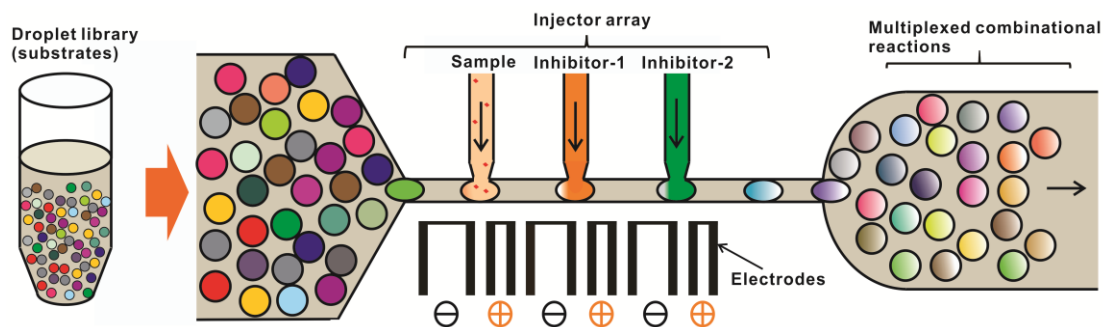
ROYAL SOCIETY OF CHEMISTRY

www.rsc.org/loc

Proteolytic activity matrix analysis (PrAMA) is a technique for simultaneously measuring multiple specific protease activities, generally requiring multiple measurements of parallel enzyme reactions combined with inhibitor analyses, and the approach is generally limited by sample quantity and the complexity of multiple reaction monitoring. To address these issues, in this study we developed a pico-injector array to generate $9*2*2*2=72$ different reactions in picoliter-sized droplets by controlling the sequence of combinational injections, which allows simultaneous read-outs of a wide range of multiple enzyme reactions and measurement of inhibitor effects by using small sample volumes.

Low-volume multiplexed proteolytic activity assay and inhibitor analysis through a pico-injector array

Ee Xien Ng[a], Miles A. Miller[b,c], Tengyang Jing[a,d], Doug A. Lauffenburger[c] and Chia-Hung Chen[a,e*]

Secreted active proteases, from families of enzymes such as matrix metalloproteinases (MMPs) and ADAMs (a disintegrin and metalloproteinases), participate in diverse pathological processes. To simultaneously measure multiple specific protease activities, a series of parallel enzyme reactions combined with a series of inhibitor analyses for proteolytic activity matrix analysis (PrAMA) are essential but limited due to the sample quantity requirements and the complexity of performing multiple reactions. To address these issues, we developed a pico-injector array to generate 72 different reactions in picoliter-volume droplets by controlling the sequence of combinational injections, which allowed simultaneous recording of a wide range of multiple enzyme reactions and measurement of inhibitor effects using small sample volumes (~10 µL). Multiple MMP activities were simultaneously determined by 9 different substrates and 2 inhibitors using injections from a pico-injector array. Due to the advantages of inhibitor analysis, the MMP/ADAM activities of MDA-MB-231, a breast cancer cell line, were characterized with high MMP-2, MMP-3 and ADAM-10 activity. This platform could be customized for a wide range of applications that also require multiple reactions with inhibitor analysis to enhance the sensitivity by encapsulating different chemical sensors.

Introduction

Proteases contribute to various pathologies and represent a family of promising drug targets and biomarker candidates. In particular, matrix metalloproteinases (MMPs) and ADAMs (a disintegrin and metalloproteinases) have been investigated as potential drug targets and diagnostic biomarkers. Metalloproteinase (MP) activities are regulated through a tight network of multiple proteolytic enzymes and inhibitors, frequently resulting in highly context-dependent behavior that has hampered their usefulness in the clinic. Existing approaches such as zymography[1], activity-based enzyme-linked immunosorbent assays (ELISAs)[2], and peptide microarrays[3] are able to perform multiplexed protease assays; however, they have been limited due to low throughput, inadequate ability to simultaneously measure multiple activities (i.e., limited multiplexing), and lack of direct kinetic measurement[4].

A recently developed analytical method, proteolytic activity matrix analysis (PrAMA), uses parallel measurements of multiple FRET-based protease sensors to infer specific enzyme activities in a non-invasive, real-time and multiplexed manner [5]. However, this approach requires a large panel of measurements in a microtiter-plate format, and consequently demands an often-restrictive amount of biological or clinical sample. Parallel testing of multiple protease inhibitors improves PrAMA specificity and accuracy, because cleavage of FRET-substrates by a given biological sample can be quantitatively compared between reactions in either the presence and absence of specific inhibitors. Unfortunately, such inhibitor analysis also increases the panel of measurements and corresponding sample requirement. Therefore, microfluidics techniques have been developed to reduce the sample requirement while increasing multiplexing ability. Droplet-based microfluidics has many significant advantages and has demonstrated potential in performing high-throughput multiplexed enzymatic assay studies[6-10]. Recently, a microfluidic pico-injector[11-13] was developed for precise fluidic control and the handling of clinical samples within water-in-oil droplets. This technology combined with a droplet library[12, 14, 15] has been shown to enable the simultaneous performance of multiple enzymatic reactions in the droplets to ascertain protease activities for diagnosis of endometriosis[4]. However, the specific droplet compositions were identified by optical barcoding using specific concentrations of available indicator dyes, which limited the number of distinct enzyme reactions that could be simultaneously assessed [14, 16, 17]. Although adopting more barcoding labels such as near-infrared dyes can potentially increase the multiplicity size, this approach requires additional optical setup complexity. Alternatively, a label-free injector array was recently demonstrated to perform large-scale multiplexed assays with hundreds of variations[18, 19], yet the complexity involved in multiple valve operations and long-term observation of reaction dynamics within droplets remain challenging[20].

To address these issues, here we introduce a pico-injector array that combines an optically-barcoded droplet library with tandem sequential injection controls to dramatically increase device multiplexing capability. We first prepared protease substrate libraries consisting of monodisperse water-in-oil droplets using droplet generator chips. The droplets were formed to encapsulate particular FRET-based fluorogenic polypeptide protease substrates, each with unique peptide sequences and corresponding protease specificities. The individual droplet compositions were distinguished by optically barcoding the droplets with specific concentrations of indicator dyes. The droplet library was then uploaded to an array with 3 pico-injectors that enabled combinatorial injections into individual droplets within the library. The pico-injectors can add a variety of useful soluble reagents to the droplets, for instance additional spectrally-distinct fluorogenic sensors or

catalysts. In this work, we use pico-injectors to add protease inhibitors for improving the quantitative accuracy of the specific protease activity measurements. Theoretically, this combinatorial tandem pico-injection enables the number of distinct, simultaneously monitored enzyme reactions to be increased from 9 to 72, all while using a small physiological sample volume (<20 μL).

The inhibitor analysis was achieved using injections of two relatively specific inhibitors for either MMP-2 or MMP-9, both of which centrally regulate various biological processes including cancer growth and metastasis [21]. After the inhibitor injections, the droplets were sent to a chamber for time-lapse reaction observations over the course of ~4 hours. The fluorescent signals inside the droplets were then imaged and computationally processed using automated software for PrAMA inference of the specific protease activities. Due to the advantages of PrAMA and inhibitor analysis, multiple protease MMP activities can be simultaneously determined. In addition to the low sample volume requirement, our platform demonstrated its advantage in characterizing the MMP/ADAM activities of MDA-MB-231, which is a breast cancer cell line with high MMP-2 activity. This work ultimately serves as a proof-of-principle for tandem pico-injectors interfacing with a barcoded droplet library, and can be extended in various ways, for instance by encapsulating different chemical sensors. The device modularity ultimately makes it highly customizable for a variety of applications that face similar issues of specificity and that could benefit from multiplexed approaches with combinatorial co-injections using limited sample amounts.

Materials and Methods

The device was fabricated as a polydimethylsiloxane (PDMS, Sylgard 184, Dow Corning Inc., Midland, MI) chip bonded to a PDMS-coated glass slide. SU-8 photoresist (SU-8-2050, MicroChem Inc., Newton, MA) was patterned on a silicon wafer to build a positive master. The positive master mold for the device contained channels that were 50 μm tall. The SU-8 master was further treated with a trichloro (1H, 1H, 2H, 2H-perfluorooctyl) silane (Sigma-Aldrich, St. Louis, MO) for 1 hour to prevent adhesion of the SU-8 features to the master mold with PDMS after molding. The trichloro (1H, 1H, 2H, 2H-perfluorooctyl) silane solution was evaporated and deposited on the master in a desiccator with a ~5 psi vacuum. In the second step, PDMS was degassed in a desiccator with a ~5 psi vacuum for 1 hour and poured on the master mold. The mold was cured in an oven at 65°C for 6 hours, and then the PDMS layer was peeled off from the silicon master. Holes were punched through the end of the channels using a Harris Uni-Core puncher with a diameter of 1.00 mm (Ted Pella, USA). To form the hydrophobic surface for making the droplet generator, a glass slide was coated with a layer of PDMS. To obtain a thin coating, the PDMS was diluted with hexane (Sigma, 1:1 mixture) and was coated on a glass slide using a spin coater at 1800 rpm. The coated glass was then placed in an oven at 65°C overnight. After plasma bonding, the device was placed in an oven at 65°C for more than 20 hours to form strong bonding

and completely hydrophobic surfaces. To fabricate the electrodes in the devices, empty microchannels in the shape of the electrodes were first constructed. The devices were heated, and a low melting-point liquid solder was injected into the empty channels. After cooling the devices, the solder was solidified to form electrodes embedded in the microfluidic devices (Supplementary-1).

The MDA-MB-231 cell line (ATCC) was cultured according to manufacturer's guidelines in DMEM supplemented with 10% FBS and penicillin-streptomycin. The cells were grown at 37°C in a humidified incubator maintained at 5% CO_2. Once 80-90% confluent, the cells were changed to serum-free medium for 24 hours prior to the collection of the supernatant. The serum-free supernatant which contained proteases secreted by the breast cancer cells were then used for a protease assay.
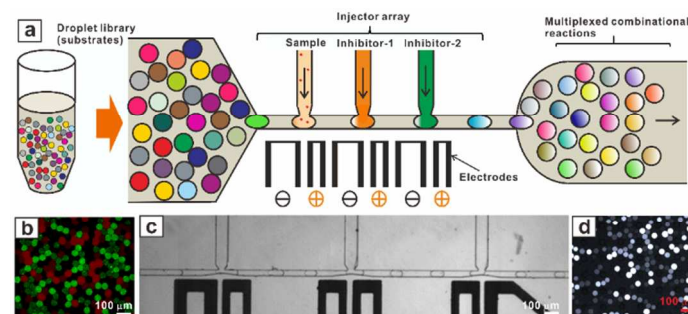

Fig. 1: (a) Schematic representation of the microfluidic device. Droplets containing various substrates are generated through a parallel droplet generator microfluidic chip and stored as a droplet library. (b) The droplet-library with fluorescent barcoding scheme. (c) A photo of the pico-injector array. (d) The reactions in the droplets with the droplets incubated in an observing chamber.

The experimental process is shown in Fig. 1a. For droplet generation, one aqueous and two oil streams were introduced into a droplet generator with a co-flow channel geometry using syringe pumps (Harvard, PHD2000). To run the droplet generator, the oil flow rate (10 μL/min) roughly matched aqueous flow rates (5 μL/min) used to form the droplets (~30 pL/droplet with a generation rate of ~4 kHz). Fluorocarbon oil HFE 7500 (3M Novec™, Singapore) with 0.5% krytox (modified) surfactant was used to generate stable, monodisperse droplets via the droplet generator microfluidic chip. 9 FRET substrates (Supplementary-2) with barcodes were individually injected through the reagent inlet of the droplet generator to form a droplet library. Each droplet had a unique concentration combination of two fluorescent indicator dyes (Alexa-405 and Alexa-546) as a barcode for labeling purposes (see Fig. 1b). The substrates were individually uploaded into the droplet generators to avoid contamination of reagents.

For pico-injection, the previously prepared droplets were passed through a narrow channel with a size similar to the droplet diameter (50 μm) at a flow rate of ~0.5 μL/min (see Fig. 1c). Oil was added from a side channel at ~1.0 μL/min to maintain the spacing between the drops for synchronization with the pico-injector. The injection process was observed

through a high-speed camera (Phantom v7.3, USA). To calibrate the pico-injector, dye-labeled samples (Alexa-488) were used to determine the ratio of injection during droplet pico-injection. The time-lapse microscopy shown in Supplementary-MV1 demonstrates the droplet pico-injection. After pico-injection, the diameter of the droplets increased, and the dilution caused by the injection contributed to a decrease in the intensity of the indicator dye (droplet intensities were processed by subtracting the background fluorescence). Based on the changes in the observed droplet volume and the indicator dye intensity, we concluded that the loading efficiency was dynamically tuned by changing the flow rates of the droplets and injectors. The applied DC voltage was ~30-50 V with a frequency of 1 kHz. The resulting droplets were then immobilized in an observing chamber for reaction screening (Fig. 1d). A time-lapse study of the droplets (Supplementary-3) was performed on a fluorescence microscope with a 4-wavelength automated excitation system (CoolLED pE-2) with a multiple bandpass filter and emitter wavelengths of 365 nm, 470 nm and 565 nm. Two of the excitation channels were used for barcode identification and one for droplet reaction tracking.
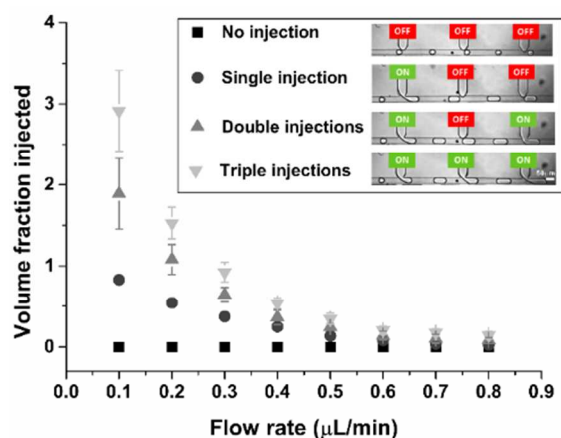
Device calibrations

Fig. 2: Injected droplet volume fraction vs droplet flow rate. As the droplet flow rate increases, less volume is injected because the contact time between the droplets and the injector nozzles decreases. The total volume injected is proportional to the number of injectors activated.

To ensure the reagent-sample ratios within the droplets for reactions, the volume injected by the pico-injector array against the inlet droplet flow rate was characterized by uploading droplets with a fluorescent indicator dye (Alexa-488, 80 μg/mL) to the injector array. The correlation between the droplet fluorescent intensity in a micro channel and the indicator dye concentration was calibrated using an sCMOS camera (Hamamatsu Orc2). The indicator dye concentrations were 20 μg/mL (179.4 ± 9.9 a.u.), 40 μg/mL (380.5 ± 31.5 a.u.), 60 μg/mL (545.6 ± 36.3 a.u.) and 80 μg/mL (801.2 ± 32.2 a.u.). The spacer oil flow rate was controlled at 1.0 μL/min, and the three injectors were set at 0.1 μL/min. The droplet flow rate

was characterized from 0.1 μL/min to 0.8 μL/min with 0.1 μL/min increments (Fig. 2). When the flow rate increased, the injected volume fraction decreased. This result could be attributed to the decrease in the contact time between the droplets and the pico-injector nozzles: when the flow rate was high, less contact time and thus less injection time were allowed at the injection point. Only limited injection was conducted above flow rates of 0.6 μL/min. The total injected volumes for the double- and triple- injectors were approximately 2x and 3x the injected volume of a single injector, respectively. We observed that the device showed better stability at higher flow rates, with 0.4-0.5μL/min giving the most stable and consistent injections (Fig. 2).

To form a droplet library with different components, the droplets were barcoded using two fluorescent indicator dyes (Alexa-405 and Alexa-546) with different concentration combinations. For each type of indicator, three sets of concentrations were prepared: 3.75 μg/mL, 7.50 μg/mL and 15.00 μg/mL, resulting in a total of 3x3=9 sets of combinations to label 9 different sets of droplets. By controlling the injection sequence of the three injectors in an injector array, a total of 2x2x2=8 different conditions can be achieved. Given the combination of the droplet library (9 sets) and the injector sequence controls (8 conditions), 9x2x2x2=72 different conditions in the droplets were demonstrated (see Fig. 3). Automated droplet tracking software written in Matlab, which was based on a modified spot-finding algorithm[22] was used to track the droplets and read the fluorescent intensities from the droplets present in the images. The tracked droplets were filtered for appropriate diameter and fluorescence continuity over time. As such, multiple large-scale reactions in the droplets were recorded to provide multiplexed information with statistical confidence.

To calibrate the reaction rates in the droplets, trypsin-substrate reactions were performed. Three sets of trypsin solutions were prepared with concentrations of 0.5x, 1x and 2x by diluting a 10x 0.5%/0.2% trypsin EDTA solution. Each trypsin solution was connected to the pico-injector array via micro-tubing (inner diameter 0.38 mm, outer diameter 1.09 mm, Scientific Commodities, USA). The droplet library with nine substrates prepared earlier was uploaded into the pico-injector array for the trypsin injections. The droplet flow rate was set to 0.5 μL/min with a spacer oil flow rate of 1 μL/min and an injector array flow rate of 0.1 μL/min to produce 10% volume injection of trypsin to the droplets. After the combinatorial injections, the droplets were collected and immobilized in observing chambers for a time-lapse study of the reaction rate. The fluorescence time lapse was set for a time period of ten minutes with 30 seconds intervals between each excitation from the CoolLED automated excitation system. The reaction rate of each substrate with trypsin showed an expected correlation with the estimated concentration after combinatorial injections (see Fig. 4 and Supplementary-4). Each substrate had a different catalytic efficiency with the trypsin protease;

however, all of the substrates followed the same pattern: higher reaction rates were obtained at higher concentrations of trypsin.
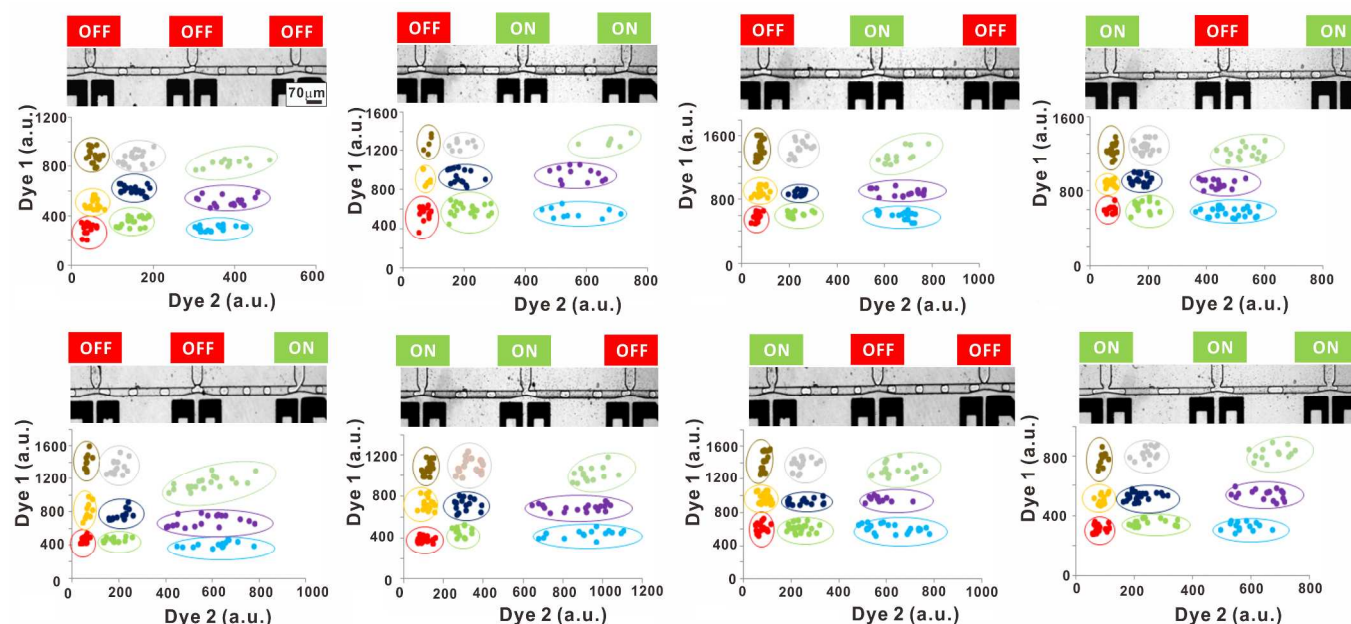

Fig. 3 A total of 72 different types of reactions can be processed by controlling the injection sequence. For each injection combination, 9 groups of substrate droplets can be identified from the library. Each dot in the above subplot corresponds to an individual droplet, categorized by color into 1 of 9 groups according to Dye-1 and Dye-2 labels, and each subplot corresponds to a unique pico-injection configuration. The similar sample-size within each droplet group is controlled by random sampling from the droplet library. Dye 1: Alexa-405; Dye 2: Alexa-546.
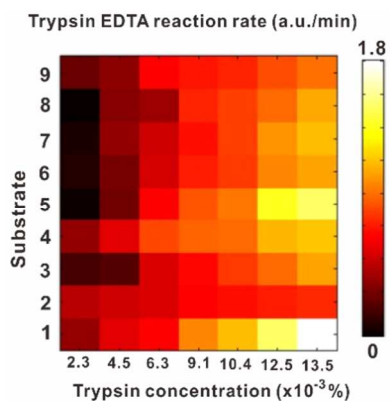

Fig. 4: Validation of the pico-injector array to increase the multiplexing capability of the assay. Seven sets of trypsin concentrations were generated from combinatorial injections. The reaction rate between each substrate and trypsin pair correlated well with the predicted concentration of trypsin after combinatorial injections.

Protease assay and inhibitor analysis

Reactions using recombinant enzymes were conducted to establish the accuracy of the microfluidic platform for inferences of specific protease activities. Purified recombinant MMP-2 and MMP-9 were injected into a barcoded droplet library consisting of 9 unique protease substrates, and PrAMA was then used to infer specific protease activity levels from the resulting data (see Fig. 5a and Fig. 5b). Sample-injected droplet fluorescence was imaged for 1.5 hours. Droplet tracking software was used to interpret the time course images, and the reaction rates were obtained from the increase in fluorescence resulting from substrate proteolysis. The 9 droplet library components were gated with three injectors to generate 72 different reaction conditions due to their unique combinations of indicator fluorescence and injection sequence (Fig. 3). The enzyme catalytic efficiencies inferred from these groupings were compared with values obtained using a standard plate reader assay ($R^2 > 83\%$ between the two assay formats). We inferred the compositions of the unknown enzyme mixtures based on their observed substrate cleavage patterns with >95% accuracy (Supplementary-5). In addition to using 9 different substrates to assay the signals from the selected proteases, several important proteases, such as MMP-2 and MMP-9, benefit from inhibitor analysis to accurately distinguish their closely related activities. Using the pico-injector array, two inhibitor analyses were conducted by introducing MMP-2 inhibitor IV and MMP-9 inhibitor I (Merck Millipore, USA) to significantly improve the accuracy. Calibration of both MMP inhibitors were conducted to investigate their inhibitory efficiency as well as cross-reactivity (Supplementary-6).

By selectively switching on and off the electric field at the inhibitor injectors, four groups of reacting droplets were generated: 1) a droplet library control group in which no inhibitors were injected into the library, 2) a droplet library injected with MMP-2 inhibitor, 3) a droplet library injected

with MMP-9 inhibitor, and 4) a droplet library injected with both MMP-2 inhibitor (concentration: 100nM) and MMP-9 inhibitor (concentration: 25nM). A mixed solution of MMP-2 and MMP-9 pure protease recombinants with a final concentration of 5 nM for each was tested. After the injections, the resulting droplets were again immobilized in observing chambers for fluorescent time-lapse studies. Fluorescent images captured with excitation at 365 nm, 565 nm (for barcoding identification) and 470 nm (for MMP activities) were obtained every 5 minutes for 3 hours. The exposure time of the camera was set to 100 ms during excitation to avoid photo-bleaching of the fluorophores. The reaction rates of each substrate in 4 conditions were calculated using Matlab software to show that when either the MMP or inhibitor was added, the reaction rates decreased as the corresponding MMP was inhibited (see Fig. 5c). As expected, the reaction rates dropped to nearly zero when both MMP inhibitors were added (Supplementary-7).
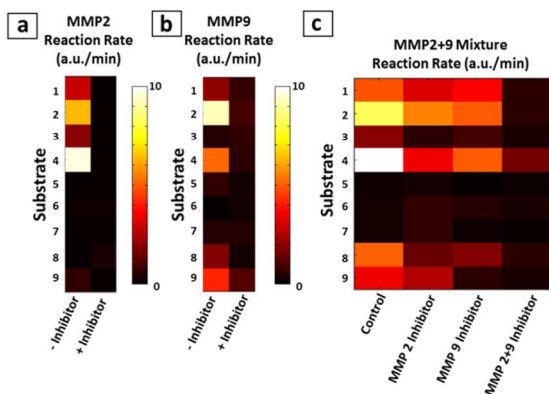

Fig. 5: (a) Reaction rates of substrates incubated with MMP-2 in the presence or absence of inhibitors. (b) Reaction rates of substrates incubated with MMP-9 in the presence or absence of inhibitors. (c) Reaction rates of substrates in 4 conditions with a mixture of recombinant MMP-2 & MMP-9. The use of MMP inhibitors caused a decrease in the reaction rates.

Physiological sample detections

After testing the purified recombinant enzymes, the pico-injector array was used to analyze a breast cancer cell line, MDA-MB-231. To ascertain the proteolytic activity of these cells, the cells were prepared in serum-free medium for 24 hours after reaching 80~90% confluency. The cells were then collected, and the supernatant was clarified. Finally, the samples were analyzed using the aforementioned droplet assay. MDA-MB-231 cells are known to highly express MMP-2 [22-24]. Furthermore, MDA-MB-231 cell migration through extracellular matrix is dependent in part on MMP-2 for its ability to cleave type IV collagen from the basement membrane [25]. MMP-9 is another protease of interest due to its similar ability to degrade extracellular matrix [26]; however, the overlapping substrate preferences of these two MMPs makes them difficult to distinguish in activity-based assays, without the use of specific inhibitors.

MDA-MB-231 supernatant was analyzed using the 9-substrate droplet library, and results showed that substrate S4 had the highest reaction rate. Control experiments with recombinant enzyme (Supplementary-5) show S4 to be preferably cleaved by MMP-2, MMP-9, and MMP-13, and therefore suggesting that these proteases could be contributing to the supernatant reaction. However, the reaction rate of the supernatant proteases with S8 and S9 was lower than what would be expected if MMP-9 or MMP-13 were present, therefore suggesting MMP-2 as the likely active enzyme.

To better distinguish MMP-2 and MMP-9, MMP inhibitors were injected into the prepared droplet library. Significant decreases in activity were observed for each pair of reaction rates with the substrates when MMP-2 inhibitor was injected, thus confirming the activity of MMP-2 in the supernatant. MMP-9 inhibitor did not greatly affect each pair of reaction rates with the substrates, which also confirmed that MMP-9 did not contribute to the final protease activities in the sample (see Fig. 6a). In agreement with these results, inference of specific protease activities using PrAMA indicated a high MMP-2 activity. The ratio of inferred MMP-2 activity in the overall activity to the fraction of effect of MMP-2 inhibitor was consistent (Supplementary-8). PrAMA additionally offered information regarding the multiple activities of MMP-3 and ADAM-10 (see Fig. 6b). MMP-3, also known as Stromelysin-1, is well known for its ability to remodel the extracellular matrix (ECM), and previous studies have found MDA-MB-231 to express MMP-3 [27, 28]. ADAM-10 is frequently overexpressed in various cancers and invasive diseases [29, 30]. It is known to be shed into the supernatant from the cell-surface [31], and is recognized as contributing to cell migration and proliferation through the shedding of ErbB growth-factor ligands (such as EGF and Amphiregulin) and receptors (such as HER2/neu) [32-34]. Although the protease activity network is still not fully understood due to its complexity, our PrAMA results suggested a few key metalloproteinases mentioned above, which could be important contributors to the invasiveness of the breast cancer cell line MDA-MB-231.
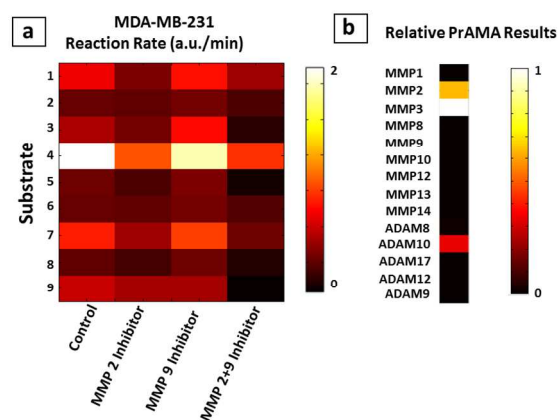

Fig. 6: (a) Reaction rates of the substrates in 4 conditions with MDA-MB-231 cell supernatant. By using MMP-2 inhibitor, the results showed that MMP-2 exists in the supernatant, which is consistent with the PrAMA inference results. In contrast,

MMP-9 inhibitor did not cause a decrease in the reaction rates, confirming that no MMP-9 was present in the supernatant. (b) PrAMA inference result of the MDA-MB-231 cell supernatant showed MMP-2 activity, as well as MMP-3 and ADAM-10 activity.

Conclusions

The integration of a pico-injector array with a barcoded droplet library exponentially increases the size of assay multiplicity through combinational injections. The multiplexing capability is important for performing both specific and broad-spectrum analysis of protease activity. PrAMA, which integrates experimental measurements and mathematical analysis, is able to consider a larger list of MMPs and ADAMs in its inference analysis given its larger droplet library. In this study, a droplet library with 9 different components was uploaded to a pico-injector array with 3 injectors to generate 9x2x2x2=72 different associations. Thousands of droplet reactions can be monitored for multiplexed assaying using small physiological sample amount (<10 μL) to assay primary clinical samples without involving cell culture steps. Due to this advantage, extensive multiple MMP/ADAM-substrate reactions and inhibitor assays in a physiological sample were simultaneously tested to enhance the accuracy of PrAMA. An inhibitor analysis was conducted to study the MMP-2 and MMP-9 activities, which are usually extremely difficult to distinguish through conventional methods. Additionally, the pico-injector array provided flexibility in the selection of inhibitors based on the detection spectrum desired. We specifically investigated multiple MMP/ADAM activities of MDA-MB-231, a breast cancer cell line, which showed high MMP-2, MMP-3 and ADAM-10 activity. In this study, the pico-injector array platform has shown its unique advantage of performing high-throughput multiplexed analyses of proteases by combining a time-lapse study of activities and PrAMA analysis. In addition to the application in protease detection, this platform could be extended by encapsulating different chemical sensors for a variety of applications that involve similar issues of specificity and that could benefit from multiplexed approaches using limited sample amounts.

Acknowledgements

Notes and references

a Department of Biomedical Engineering, National University of Singapore, 9 Engineering Drive 1, Singapore 117575, Singapore

b Center for Systems Biology, Massachusetts General Hospital, Boston, MA 02114, USA

c Department of Biological Engineering, Massachusetts Institute of Technology, Cambridge, MA02139, USA

d Singapore-MIT Alliance for Research and Technology (SMART) Centre, Singapore 1385602, Singapore

e Singapore Institute for Neurotechnology (SINAPSE), 5F, 28 Medical Drive, Singapore 117456, Singapore

.

References

1   D.E. Kleiner and W.G. Stetler-Stevenson, Anal. Biochem., 1994, 218, 325-329.

2   . J.L. Lauer-Fields, H. Nagase and G.B. Fields, J. Biomol. Technol., 2004, 15, 305-316.

3   D.N. Gosalia, W.S. Denny, C.M. Salisbury, J.A. Ellman and S.L. Diamond, Biotechnol. Bioeng., 2006, 94, 1099-1110.

4   C.H. Chen, M.A. Miller, A. Sarkar, M.T. Beste, K.B. Isaacson, D.A. Lauffenburger, L.G. Griffith and J. Han, J. Am. Chem. Soc., 2013, 135, 1645-1648.

5   M.A. Miller, L. Barkal, K. Jeng, A. Herrlich, M. Moss, L.G. Griffith and D.A. Lauffenburger, Integr. Biol., 2011, 3, 422-438

6   A. Huebner, L.F. Olguin, D. Bratton, G. Whyte, W.T.S. Huck, A.J. de Mello, J.B. Edel, C. Abell and F. Hollfelder, Anal. Chem., 2008, 80, 3890-3896.

7   H. Song, D.L. Chen and R.F. Ismagilov, Angew. Chem. Int. Ed., 2006, 45, 7336-7356.

8   T.D. Rane, H.C. Zec and T. Wang, 17th International Conference on Miniaturized Systems for Chemistry and Life Sciences, 2013, 1595-1597.

9   C. Chang, J. Sustarich, R. Bharadwaj, A. Chandrasekaran, P.D. Adams and A.K. Singh, Lab Chip, 2013, 13, 1817-1822.

10 H.N. Joensson, M.L. Samuels, E.R. Brouzes, M. Medkova, M. Uhlén, D.R. Link and H. Andersson-Svahn, Angew. Chem. Int. Ed., 2009, 48, 2518-2521

11 H.N. Joensson, M.L. Samuels, E.R. Brouzes, M. Medkova, M. Uhlén, D.R. Link and H. Andersson-Svahn, Angew. Chem. Int. Ed., 2009, 48, 2518-2521.

12 M.T. Guo, A. Rotem, J.A. Heyman and D.A. Weitz, Lab Chip, 2012, 12, 2146-2155.

13 A.R. Abate, T. Hung, P. Mary, J.J. Agresti and D.A. Weitz, Proc. Natl. Acad. Sci., 2010, 107, 19163-19166.

14 E. Brouzes, M. Medkova, N. Savenelli, D. Marran, M. Twardowski, J.B. Hutchison, J.M. Rothberg, D.R. Link, N. Perrimon and M.L. Samuels. Proc. Natl. Acad. Sci., 2009, 106, 14195-14200.

15 T.S. Kaminski, S. Jakiela, M.A. Czekalska, W. Postek and P. Garstecki, Lab Chip, 2012, 12, 3995-4002.

16 R. Dangla, S.C. Kayi and C.N. Baroud, Proc. Natl. Acad. Sci., 2013,110, 853-858.

17 M. Han, X. Gao, J. Z. Su and S. Nie, Nat. Biotechnol., 2001, 19, 631–635.

18 H.C. Zec, T.D. Rane, W. Chu, V.W. Wang and T. Wang, MEMS, 2013 IEEE 26th International Conference, 2013, 263-266.

19 H. Zec, T.D. Rane, T. Wang, Lab Chip, 2012, 12, 3055-3062.

20 S.R. Head, H.K. Komori, S.A. LaMere, T. Whisenant, F. Van Nieuwerburgh, D. R. Salomon and P. Ordoukhanian, BioTechniques, 2014, 56, 61-77.

21 G. Klein, E. Vellenga, M.W. Fraaije, W.A. Kamps and E.S.J.M. de Bont, Oncology Hematology, 2004, 50, 87-100.

22 A. Santella, Z. Du, S. Nowotschin, A.K. Hadjantonakis and Z. Bao, BMC Bioinformatics, 2010, doi: 10.1186/1471-2105-11-580.

23 O. Baum, R. Hlushchuk, A. Forster, R. Greiner, P. Clézardin, Y. Zhao, V. Djonov and G. Gruber, Int. J. Oncol., 2007, 30, 325-332.

24 T. Yuan, Y. Wang, Z.J. Zhao, H. Gu, J. Biol. Chem., 2010, 285, 14861-14870.

25 Moulik S, Pal S, Biswas J, Chatterjee A, J. Tumor, 2014, 2(2), 87-98.

26 S.B. Kondapaka, R. Fridman and K.B. Reddy, Int. J. Cancer, 1997, 70, 722-726.

27 S. Moulik, T. Sen, A. Dutta, A. Banerji, C. Ghosh, S. Das and A. Chatterjee, J. Cancer Mol, 2008, 4, 55-60.

28 K. Phromnoi, S. Yodkeeree, S. Anuchapreeda and P. Limtrakul, Nature APS, 2009, 30, 1169-1176.

29 M. Balduyck, F. Zerimech, V. Gouyer, R. Lemaire, B. Hemon, G. Grard, C. Thiebaut, V. Lemaire, E. Dacquembronne, T. Duhem, A. Lebrun, M. Dejonghe and G. Huet, Clinical & Experimental Metastasis, 2000, 18, 171-178.

30 M.L. Moss, A. Stoeck, W. Yan and P.J. Dempsey, Current Pharmaceutical Biotechnology, 2008, 9, 2-8.

31 D.R. McCulloch, P. Akl, H. Samaratunga, A.C. Herington and D.M. Odorico, Clinical Cancer Research, 2004, 10, 314-323.

32 M.L.Moss, G. Powell, M.A. Miller, L. Edwards, B. Qi, Q.A. Sang, B.D. Strooper, I. Tesseur, S.F. Lichtenthaler, M. Taverna, J.L. Zhong, C. Dingwall, T. Ferdous, U. Schlormann, P. Zhou, L.G. Griffith, D.A. Lauffenburger, R. Petrovich and J.W. Bartsch, J. Biol. Chem. 2011, 286, 40443-40451.

33 M.A. Miller, A.S. Meyer, M.T. Beste, Z. Lasisi, S. Reddy, K.W. Jeng, C.H. Chen, J. Han, K. Isaacson, L.G. Griffith and D.A. Lauffenburger, PNAS, doi: 10.1073/pnas.1222387110.

34 Z. Mitri, T. Constantine and R. O'Regan, Chemotherapy Research and Practice, 2012, 20, doi:10.1155/2012/743193.

35 P. Liu, X. Liu, Y. Li, M. Covington, R. Wynn, R. Huber, M. Hillman, G. Yang, D. Ellis, C. Marando, K. Katiyar, J. Bradley, K. Abremski, M. Stow, M. Rupar, J. Zhuo, Y. Li, Q. Lin, D. Burns, M. Xu, C. Zhang, D. Qian, C. He, V. Sharief, L. Weng, C. Agrios, E. Shi, B. Metcalf, R. Newton, S. Friedman, W. Yao, P. Scherle, G. Hollis, T. Burn, Cancer Biology & Therapy, 2006, 5:6, 657-664.